Supporting Information

Metal-free Cysteamine Functionalized Graphene Alleviates Mutual Interferences in Heavy Metals Electrochemical Detection

*Qiuyue Yang, Emily P. Nguyen, David Panáček, Veronika Šedajová, Vítězslav Hrubý, Giulio Rosati, Cecilia de Carvalho Castro Silva, Aristides Bakandritsos, Michal Otyepka, and Arben Merkoçi**

Heavy metal pollutants are of great concern to environmental monitoring due to their potent toxicity. Electrochemical detection, one of the main techniques, is hindered by the mutual interference of various heavy metal ions in practical use. In particular, the sensitivity of carbon electrodes to Cd^{2+} ions (one of the most toxic heavy metals) is often overshadowed by some heavy metals (e.g. Pb^{2+} and Cu^{2+}). To mitigate interference, metallic particles/films (e.g. Hg, Au, Bi, Sn) are typically required to be embedded in the carbon electrodes. However, these additional metallic matters may face issues of secondary pollution and unsustainability. In this study, a metal-free and sustainable nanomaterial, cysteamine covalently functionalized graphene (GSH), is found to enhance a 6-fold boost in Cd^{2+} sensitivity of screen-printed carbon electrodes (SPCE), while the sensitivities to Pb^{2+} and Cu^{2+} are not influenced in simultaneous detection. The selective enhancement could be attributed to the grafted thiols on GSH sheets, with good affinity to Cd^{2+} ions based on Pearson's Hard and Soft Acid and Base Principle. More intriguingly, the GSH-modified SPCE (GSH-SPCE) features high reusable cycling times (23 times), surpassing the state-of-art SPCEs modified by non-covalently functionalized graphene derivatives. Lastly, the GSH-SPCE is validated in tap water.

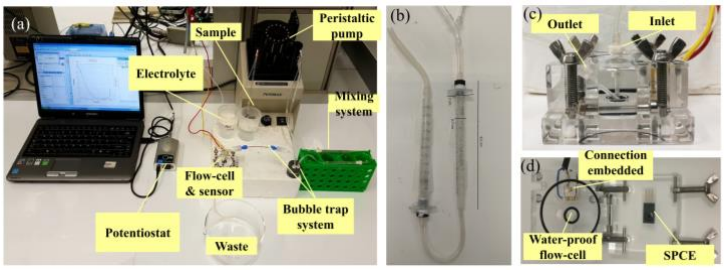

Figure S1. Photo of the fluidic sensing system used in our study. The photo of (a) the fluidic sensing system for optimization, and all heavy metal (HM) detection analysis, (b) homemade mixers (12 cm×4 cm) including two syringes (d=6 mm) with PDMS particles filling inside. (c) the encapsulated flowcell with the size of 6 cm×6 cm×3 cm including 4 screws, two pieces of PMMA, one inlet and one outlet, and (d) the open flowcell with two o-rings with a diameter of 42 mm, and 8mm respectively, which limits the flow and provides a stable chamber (~50 μL) for electrochemical reaction and customized embedded electronic connection with SPE and mini-potentiostat.

Fluidic sensing system

The fluidic heavy metal detection system was used for *in-situ* and automatic HM detection including a peristaltic pump, a mixing system, a bubble trap, a customized flowcell (including one SPCE), a mini-potentiostat (Emstat4, Palmsens) and a portable computer. The sample and electrolyte were moved by the peristaltic pump and mixed by the mixing system. Any invading bubbles can be expelled by degasser to prevent any interference in flowcell. The flowcell consisted of two o-rings making an encapsulated space for the chemical reaction on the surface of SPCE in the flowcell. Besides, there was an electronic connector embedded in the flow cell. It is connected to the mini-potentiostat which transmits the electrochemical signals to the laptop or other data analyzers like mobile phones and tablets. During the deposition step, the pump started to move the sample and electrolytes to the surface of SPCE, which can accumulate and reduce the target cations to metals. Then, the flow was stopped, and the electrochemical cell reached the equilibrium step and stripping step. After the stripping step, the obtained voltammogram can be visualized and analyzed on the portable computer.

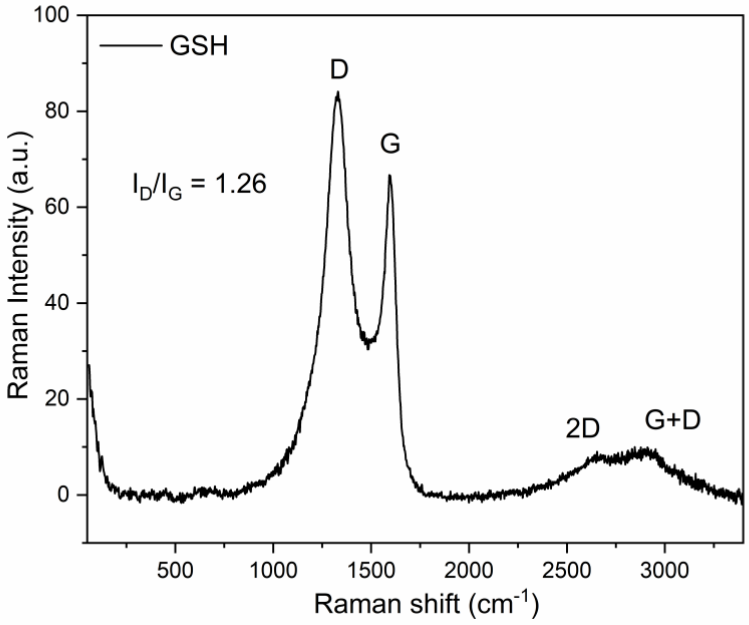

Figure S2: Raman spectrum of GSH nanosheet

Optimization results for GSH-SPCE testing conditions

The type of supporting electrolyte and its concentration, flow rate, flow time, and deposition time were optimized. Each of them and the amount of GSH added to the devices have been optimized with a one-variable-at-a-time approach.

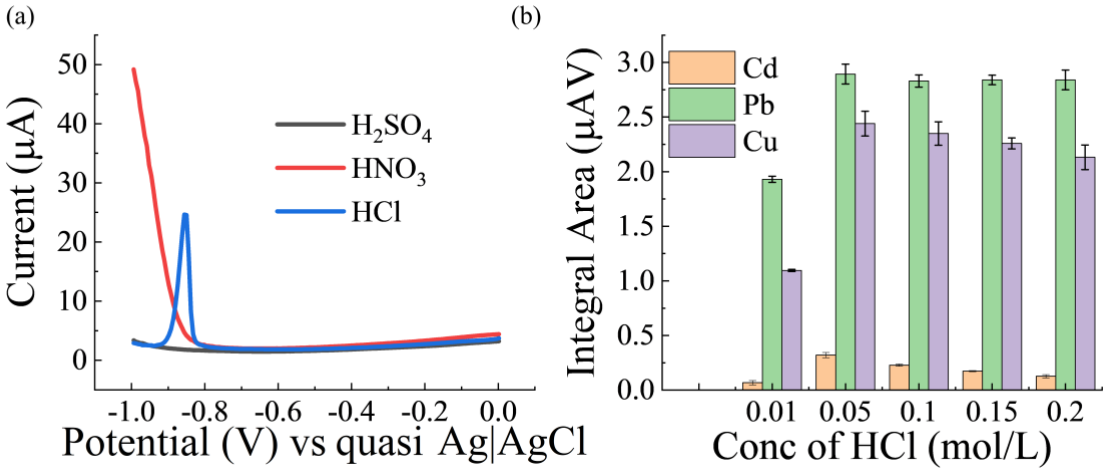

Figure S3. Optimization of different supporting electrolytes and concentrations (a) The GSH-SPCE voltammogram of 80 ppb Cd in different supporting electrolytes of 0.05 M HCl, 0.05 M HNO_3 and 0.025 M H_2SO_4. (b) GSH-SPCE were tested in 80 ppb Cd, Cu and Pb with various concentrations of HCl (0.01, 0.05, 0.1, 0.15 and 0.2 M). 0.05 M HCl was selected for the best performance.

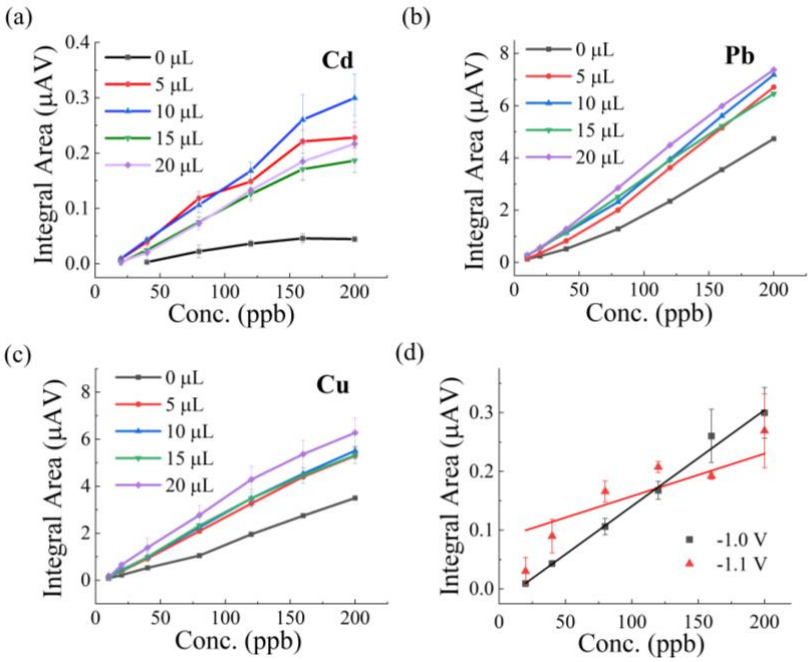

Figure S4. Optimization of different volumes of GSH supernatant drop-casted on SPCEs and deposition potential. The bare SPCE modified by different volumes of GSH supernatant was tested in various concentrations of Cd, Pb and Cu (1:1:1). The tested signals with varied HM concentrations of (a) Cd, (b) Pb and (c) Cu. The sensitivities/slopes of Cd from 0 to 20 µL were 0.0003, 0.0013, 0.0017, 0.0011, and 0.0012 µAV·ppb^{-1}, respectively. The sensitivities of Pb from 0 to 20 µL were 0.024, 0.035, 0.036, 0.033, and 0.0381 µAV·ppb^{-1}, respectively. The sensitivities of Cu from 0 to 20 µL were 0.018, 0.028, 0.029, 0.028, and 0.033 µAV·ppb^{-1}, respectively. 10 µL was selected for the best Cd signals. (d) The calibration curve of Cd in a mixed solution of Cd, Pb, and Cu (1:1:1) with different deposition potentials (-1 V and -1.1 V). -0.9 V was also tested, however, due to the largely negative potential that Cd^{2+} requires, no observable sensing signal of Cd^{2+} can be obtained and thus, it is not demonstrated in Figure S3d.

Table S1 The detailed data in optimization of different deposition potentials. Detailed sensitivity and R-square of Cd, Pb and Cu in the calibration during different deposition potentials of -1V and -1.1V. -1.0 V was selected for better slope and linearity.

		-1.0 V	-1.1 V
Cd	Slope	0.0017	0.0012
	R^2	0.993	0.8888
Pb	Slope	0.0364	0.0369
	R^2	0.9951	0.9716
Cu	Slope	0.0287	0.0264
	R^2	0.9982	0.9755

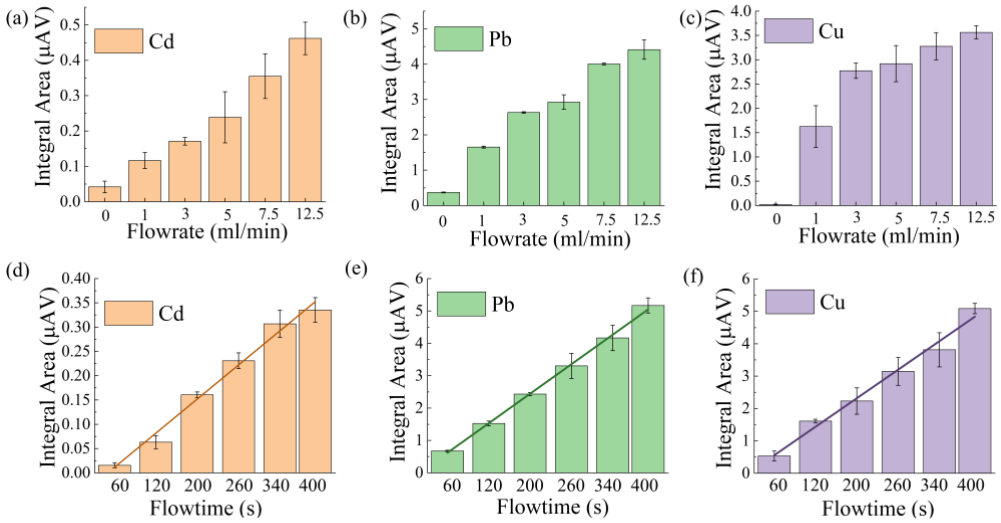

Figure S5. Optimization of flow time and flow rate. The GSH-SPCE signal diagram of (a) Cd, (b) Pb, and (c) Cu in the mixed 80ppb Cd, 80ppb Pb and 80ppb Cu solution with different flowrate. 3 mL/min was selected for Pb and Cu signals not increasing much with a higher flow rate. The GSH-SPCE signal diagram of (d) Cd, (e) Pb, and (f) Cu in the mixed 80ppb Cd, 80ppb Pb and 80ppb Cu solution with different flow time (deposition time). 200 s was selected for a mediate sensing signal with rapid sensing time.

Calibrations of Cd^{2+}, Pb^{2+} and Cu^{2+} in their individual solutions

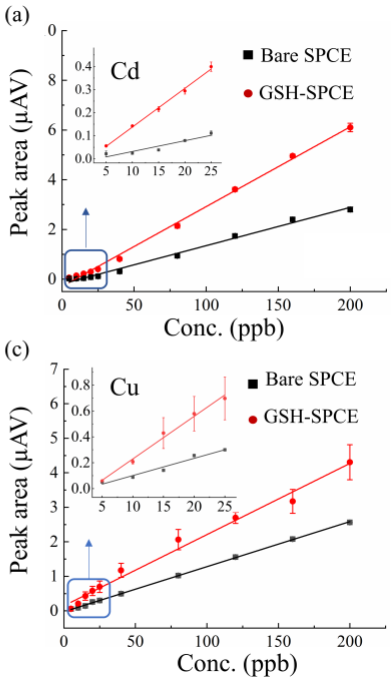

(d)

		Bare SPCE	GSH-SPCE
Sensitivity (μAV/ppb)	Cd	0.015	0.032
	Pb	0.0054	0.021
	Cu	0.013	0.021
LOD (ppb)	Cd	18.34	5.36
	Pb	19.20	3.49
	Cu	1.91	3.61

Figure S6. The individual HM ions detection. The calibration curves to (a) Cd, (b) Pb and (c) Cu of GSH-SPCE (red) and bare SPCE (black). (d) The detailed sensitivity and LOD in bare SPCE and GSH-SPCE.

The GSH-SPCE and bare SPCE were studied by Cyclic Voltammetry (CV) and Electrochemical Impedance Spectrometry (EIS)

The GSH-SPCE and bare SPCE were used to perform CV and electrochemical impedance spectroscopy (EIS) with a standard potentiostat (PGSTAT12, Autolab) in 0.01 M Ferro/Ferricyanide in 0.1 M KCl. The SPCEs were tested by EIS with the applied potential of E0. The measurements were performed in the 1 Hz -10 kHz frequency range, 10 points per decade. EIS data were fit with the Randle equivalent circuit using Zview 2® software (Scribner and Associates).

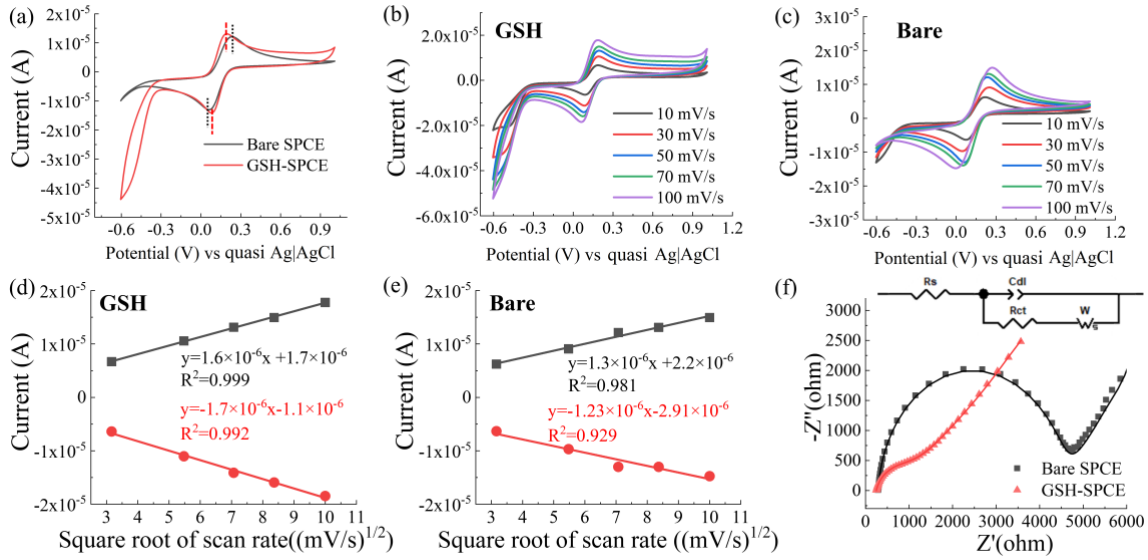

Figure S7. Cyclic voltammetry and electrochemical impedance spectroscopy of Bare and GSH-SPCE. (a) Cyclic voltammetry (CV) of GSH-SPCE and bare SPCE in 0.01 M $[Fe(CN)_6]^{4-/3-}$ in 0.1 M KCl at the scan rate of 50 mV/s. Cyclic voltammetry of (b) GSH-SPCE and (c) bare SPCE in 0.01 M $[Fe(CN)_6]^{4-/3-}$ in 0.1 M KCl at a different scan rate of 10, 30, 50, 70, and 100 mV/s. The regression line of the peak current (A) and the square root of the scan rate $((mV/s)^{1/2})$ of (d) GSH-SPCE (Anodic: $y=1.6\times10^{-6}X+1.7\times10^{-6}$ $R^2=0.999$; Cathodic: $y=-1.7\times10^{-6}-1.1\times10^{-6}$ $R^2=0.992$), and (e) bare SPCE (Anodic: $y=1.3\times10^{-6}x+2.2\times10^{-6}$ $R^2=0.981$; Cathodic: $Y=-1.2\times10^{-6}-2.1\times10^{-6}$ $R^2=0.929$). The electroactive area of GSH-SPCE, calculated by the Randles-Sevcik equation, was found to be 1.34 times larger than the one of bare SPCE (5.44 cm^2). (f) The electrochemical impedance spectroscopy (EIS) data (dots) and fitting (lines) of GSH-SPCE and bare SPCE in 0.01 M $[Fe(CN)_6]^{4-/3-}$ in 0.1 M KCl. The detailed fitting results are shown in Table S3.

Table S2. The detailed fitting results in electrochemical impedance spectroscopy

	Chi-Sqr	Sum-Sqr	Rs(+)	Rs(Error%)	Cdl-T(+)	Cdl-T(Error%)	Rct(+)
Bare	0.00015	0.017	288.60	0.29	1.1E-06	1.79	4255.00
GSH	5.11E-05	0.0059	245.50	0.17	1.52E-05	3.15	809.90
	Rct(Error %)	**W-R(+)**	**W-R(Error%)**	**W-T(+)**	**W-T(Error%)**	**W-P(+)**	**W-P(Error%)**
Bare	0.59	9458.00	12.64	12.86	19.60	0.59	2.26
GSH	2.07	10590.00	6.70	16.20	13.02	0.46	0.81

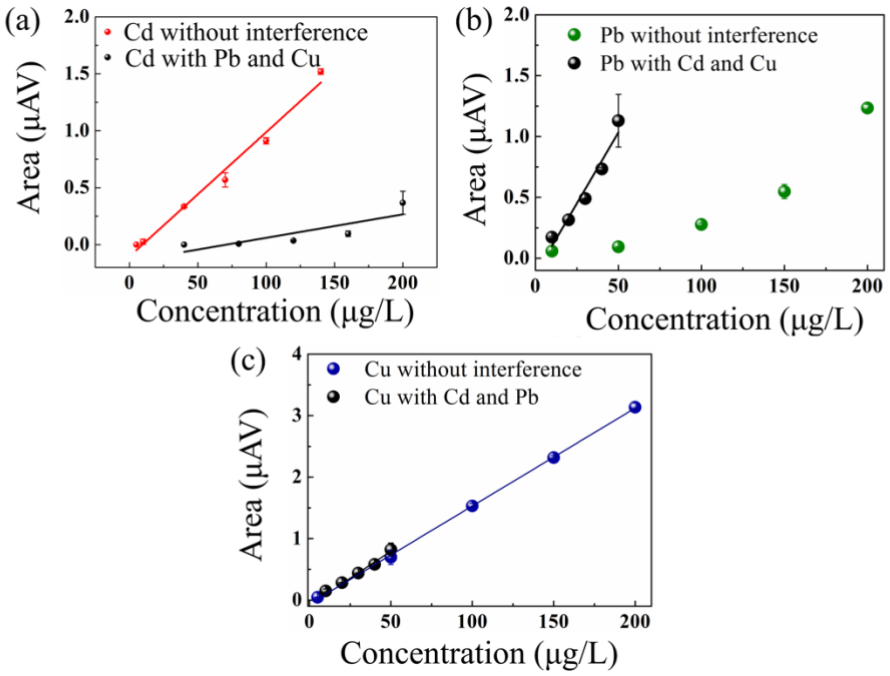

Figure S8. The comparison between individual measurements and simultaneous measurements on bare SPCE in our previous study.[1] It was shown a dramatic drop in Cd sensitivity by the mutual interference of Pb and Cu.

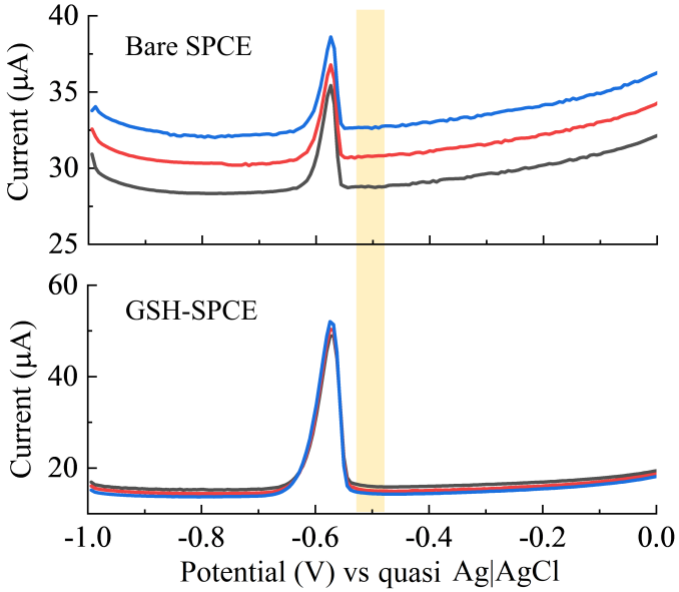

Figure S9. The absence of peak B in individual detection of 80 ppb Pb. The voltammograms of bare SPCE and GSH-SPCE were tested in the individual 80 ppb Pb solution. The stripping curves with different colours were obtained in three continuous measurements by a single electrode (n=3). The yellow background highlighted the absence of peak B in Figure 3(d-e) in the manuscript

Table S3. The summary of the obtained sensitivity (calibration slope), Y-intercept and R^2 in all comparative experiments in this study.

HMs	Various concentrations of Cd	SPCEs	Sensitivity (µAV/ppb)	Y intercept (µAV)	R^2
Cd	Individual measurement	GSH	0.032	-0.29	0.996
		Bare	0.015	-0.19	0.990
	With 80 ppb Pb	GSH	0.0066	-0.077	0.995
		Bare	0.00053	-0.010	0.971
	With 80 ppb of Cu and Pb	GSH	0.0038	-0.12	0.928
		Bare	-	-	-
	Simultaneous measurement	GSH	0.0017	-0.024	0.991
		Bare	0.00027	-0.0018	0.841
	Various concentration of Pb	**SPCEs**	**Sensitivity (µAV/ppb)**	**Y intercept**	**R^2**
Pb	Individual measurement	GSH	0.021	-0.023	0.998
		Bare	0.0054	-0.10	0.959
	With 80 ppb Cd	GSH	0.022	-0.16	0.995
		Bare	0.0056	-0.14	0.918
	With 80 ppb Cd and Cu	GSH	0.033	0.22	0.999
		Bare	0.028	0.28	0.995
	Simultaneous Measurement	GSH	0.036	-0.27	0.994
		Bare	0.024	-0.36	0.982
	Various concentration of Cu	**SPCEs**	**Sensitivity (µAV/ppb)**	**Y intercept**	**R^2**
Cu	Individual measurement	GSH	0.021	0.15	0.984
		Bare	0.013	-0.026	0.999
	With 80 ppb of Cd	GSH	0.034	0.19	0.988
		Bare	0.033	0.10	0.994
	With 80 ppb of Pb and Cd	GSH	0.032	-0.22	0.999
		Bare	0.028	-0.16	0.999
	Simultaneous measurement	GSH	0.029	-0.10	0.997
		Bare	0.018	-0.19	0.992

Table S4. The LODs of GSH-SPCE and bare SPCE towards Cd, Pb and Cu in the simultaneous detection

	Cd	Pb	Cu
Bare SPCE	84 ppb	18 ppb	12 ppb
GSH-SPCE	15 ppb	11 ppb	6 ppb

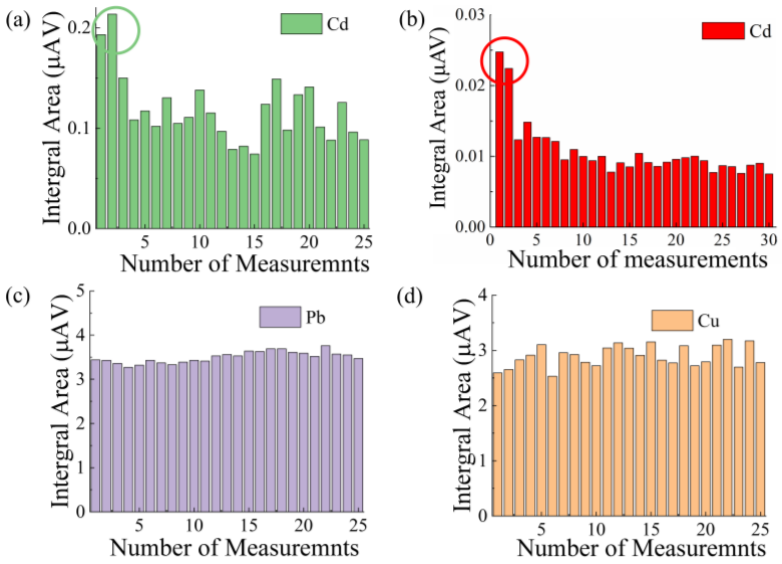

Figure S10. The data of sensing signals in repeatability study. The diagram of one GSH-SPCE in the mixed solution of 80 ppb (a) Cd, (c) Pb, and (d) Cu with continuous 25 measurements for 150 min. (b) The signal diagram of the bare SPCE in the mixed solution of 80 ppb Cd, Pb, and Cu with continuous measurements.

Table S5. Summary of reusable times and repeatability in other studies using Bi-based electrodes and non-covalently functionalized graphene derivatives/composites

Electrode	Target	Cyclin-g times	RSD (%) *or* Stability (% of initial response)				REF
			Cd^{2+}	Pb^{2+}	Cu^{2+}	Other ions	
Nanoporous Bi modified CPE	Cd^{2+}, Pb^{2+}	40	RSD=3.1%	RSD=4.3%	-		2
Bi modified CPE	Cd^{2+}, Pb^{2+}	12	RSD=5.6%	RSD=6.0%	-		3
Bi/rGO modified CPE	Cd^{2+}, Pb^{2+}	6	RSD=2.5%	RSD=2.5%	-		4
BiNPs modified GCE BiNPs/3D graphene modified GCE	Cd^{2+}, Pb^{2+}	5 16	RSD=16.85% RSD=2.43%	RSD=14.13% RSD=2.11%	-		5
Bi/IL/rGO modified SPCE	Cd^{2+}, Pb^{2+}	5	RSD=3.6%	RSD = 2.8%	-		6
Nafion/Bi/IL/graphen-e modified on SPCE	Zn^{2+}, Cd^{2+}, Pb^{2+}	10	RSD≤8%	RSD≤8%	-	RSD≤8% (Zn^{2+})	7
Bismuthene modified SPCE	Cd^{2+}, Pb^{2+}	5	RSD=4.2%	RSD= Pb^{2+}	-		8
Tryptophan modified rGO dropcasted on GCE	Cu^{2+}	10	-	-	RSD=2.13%		9
DTT/GO/Nafion modified SPCE	Cd^{2+}, Pb^{2+}, Cu^{2+}, Hg^{2+}	2 3	Stability=70% Stability=30%	Stability=70% Stability=30%	Stability=70% Stability=30%	Stability=70% (Hg^{2+}) Stability=30% (Hg^{2+})	10
COF-SH/graphene/Nafion dropcasted GCE	Cd^{2+}, Pb^{2+}, Cu^{2+}, Hg^{2+}	6	RSD<5%	RSD<5%	RSD<5%	RSD<5% (Hg^{2+})	11
Graphene/PANI modified SPCE	Zn^{2+}, Cd^{2+}, Pb^{2+}	10	RSD<11%	RSD<11%	-	RSD<11% (Zn^{2+})	12
rGO/Brominated PANI dropcasted GCE	Cd^{2+}, Pb^{2+}	10	RSD=3.16%	RSD= 2.96%	-		13
ABT/rGO/nickel ferrite modified GCE	Cd^{2+}, Cu^{2+}, Hg^{2+}	6	RSD=1.7%	-	RSD=2.6%	RSD=1% (Hg^{2+})	14
Ppy/rGO hydrogel modified GCE	Pb^{2+}	5	-	Stability=94%	-		15
Pyrrole/3D graphene aerogel modified GCE	Cd^{2+}	10	RSD=2.4%	-	-		16

Electrode	Target	Cyclin-g times	RSD (%) or Stability (% of initial response)				REF
			Cd^{2+}	Pb^{2+}	Cu^{2+}	Other ions	
Salicylaldehyde - Cysteine ligand/AuNPs/rGO modified GCE	Cd^{2+}, Pb^{2+}	10	RSD=2.4%	RSD= 2.2%	-		17
g-C_3N_4/rGO modified GCE	Pb^{2+}	7	-	RSD=3.2%	-		18
GDY/Graphene modified GCE	Cd^{2+}, Pb^{2+}	10	RSD=2.09%	RSD=1.48%	-		19
Fc/Chitosan/graphene modified graphene electrode	Cd^{2+}, Pb^{2+}, Cu^{2+}	1		Disposal device			20
Quercertin/rGO modified graphite electrode	Cd^{2+}, Pb^{2+}	5	RSD=3.5%	RSD=3.5%	-		21
Aptamer/g-C_3N_4/rGO modified GCE	Cd^{2+}	7	Stability=80 %	-	-		22
Nafion/Calcium lignosulphonate/porous graphene modified GCE	Cd^{2+}, Pb^{2+}	8	RSD=4.54%	RSD=3.63%	-		23
NH_2-MIL-88(Fe)/rGO GCE	Cd^{2+}, Pb^{2+}, Cu^{2+}	5	RSD=3.13%	RSD=0.90%	RSD=2.46%		24
GSH modified SPCE	Cd^{2+}, Pb^{2+}, Cu^{2+}	23	RSD=20%	RSD=3.68%	RSD=6.69%		This study

CPE: Carbon Paste Electrode

BiNPs: Bismuth Nanoparticles

IL: Ionic Liquid

DTT: Diaminoterthiophene

ABT: 2-(Anthracen-9-yl)benzothiazole

Ppy: Polypyrrole

GDY:Graphdiyne

Table S6. The data of sensitivities in reproducibility study and Student´s T-test. The sensitivities of 5 GSH-SPCEs (group GSH) and 5 bare SPCEs (group Bare) were operated by Student's T-test to investigate the static difference between group GSH and group Bare.

Group GSH	Group bare	Group GSH	Group bare	Group GSH	Group bare
Cd Sensitivity (μAV/ppb)		Pb Sensitivity (μAV/ppb)		Cu Sensitivity (μAV/ppb)	
0.0012	0.0003	0.032	0.029	0.045	0.046
0.0014	0.0002	0.026	0.029	0.041	0.042
0.0018	0.0003	0.035	0.028	0.046	0.044
0.0011	0.0002	0.030	0.029	0.045	0.045
0.0014	0.0002	0.029	0.030	0.046	0.046

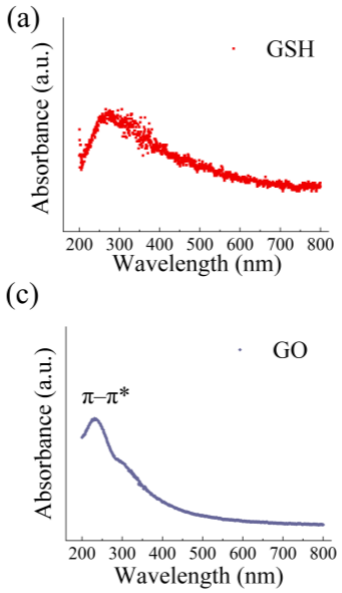

(d)

	GSH	GA	GO
Absorbance @660 nm	0.011	0.0092	0.0076
Concentration (mg/ml)	0.016	0.013	0.011

Figure S11. The estimated concentration of GSH, GA and GO is characterized by UV-Vis. The UV-Vis spectra of the obtained graphene supernatants *i.e.*, (a) GSH, (b) GA and (c) GO after adapting the concentration with GSH by dilution. (d) The table of estimated concentrations of graphene derivatives using UV-Vis by the Beer-Lamber equation is reported elsewhere.[25]

Table S7. Typical hard and soft acids and bases example [26,27]

Hard acids	H^+, Na^+, K^+, Mg^{2+}, Ca^{2+}
Hard bases	RNH_2, ROH, RCOOH
Soft acids	Cd^{2+}, Hg^{2+}, Pt^{2+}, Pd^{2+}
Soft bases	R_2S, RSH, RS^-
Intermediate acids	Pb^{2+}, Cu^{2+}, Zn^{2+}, Fe^{2+}, Ni^{2+}
Intermediate bases	$C_6H_5NH_2$

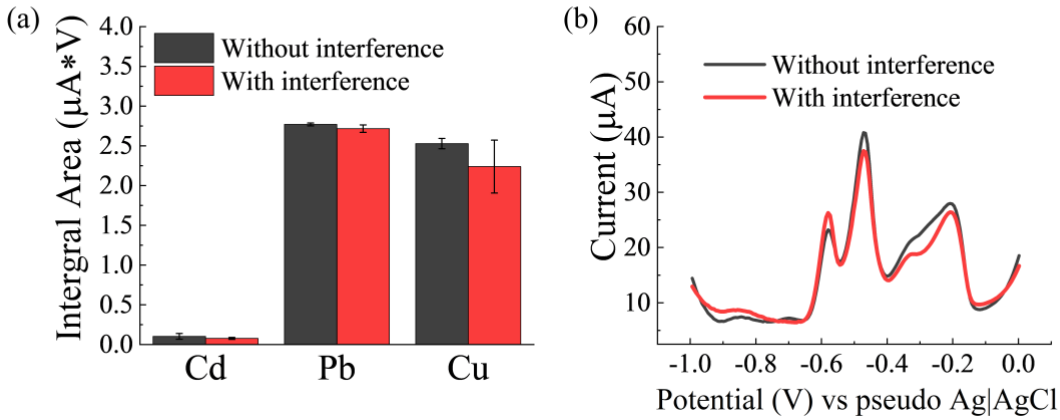

Figure S12. The detailed data in the interference study. HM responses (the peak areas from voltammograms in b) of the GSH-SPCE to be tested in the mixed solution containing 80 ppb Cd^{2+}, 80 ppb Pb^{2+} and 80 ppb Cu^{2+} (black, without interference) and in the mixed solution of 80 ppb Cd^{2+}, 80 ppb Pb^{2+} and 80 ppb Cu^{2+} with the other interferents (400 ppb of Na^{+}, K^{+}, Ca^{2+}, Mg^{2+}, Ni^{2+}, Zn^{2+}, As^{3+} and Hg^{2+}).

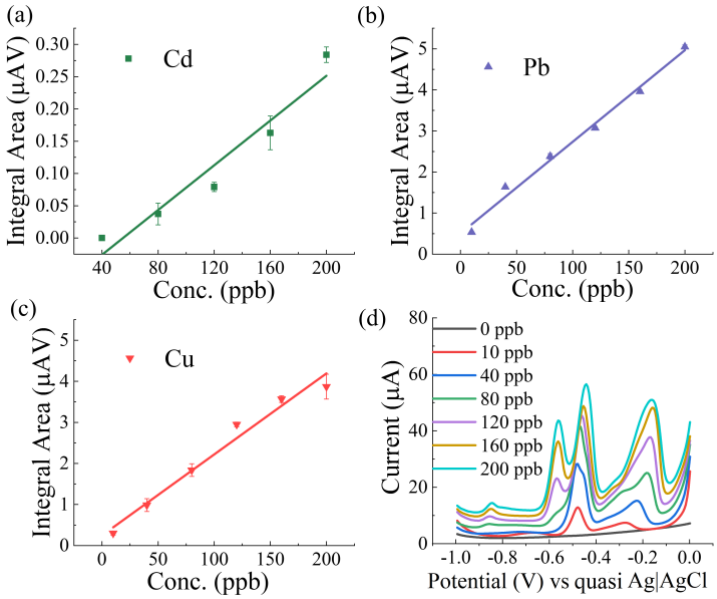

Figure S13. The sensing performance of GSH-SPCE in spiked tap water. The calibration of (a) Cd, (b) Pb, and (c) Cu by GSH-SPCE in spiked tap water with different concentrations of Cd, Pb and Cu (1:1:1). The calibration curve of Cd, Pb, and Cu is y=0.0017x-0.095 R^2=0.936, y=0.022x+0.50 R^2=0.989, and y=0.019x+0.25 R^2=0.974 respectively. (d)The voltammograms of spiked tap water by GSH-SPCE from 0 to 200 ppb.

Table S8 The investigation of the accuracy of GSH-SPCE in spiked tap water. Recovery of mixed 90 ppb Cd^{2+}, Pb^{2+} and Cu^{2+} in simultaneous detection

	Spiked conc. HMs (ppb)	Calculated Conc.(ppb)	SD (ppb)	Recovery (%)	Conc. tested by ICP-MS (ppb)
Cd^{2+}	90	73.5	5.03	81.63	92
Pb^{2+}	90	73.4	1.79	81.61	94
Cu^{2+}	90	72.3	4.70	80.31	94

Table S9. Comparison with other studies in the literature

Functional materials	Electrodes	Cd Sensitivity	Cd LOD	Pb Sensitivity	Pb LOD	Cu Sensitivity	Cu LOD	Metal - free	Detection type	REF
Bismuthene	SPCE	2.32 (nAV/ppb)	0.06 ppb	2.76 (nAV/ppb)	0.07 ppb	-	-	No	Simultaneous	8
rGO/Brominated PANI	GCE	4547.77 (μA/μM)	0.73 ppb	3914.01 (μA/μM)	1.51 ppb	-	-	Yes	Simultaneous	13
Graphene	Laser scribed PI	-	-	-	15.00 ppb	-	-	Yes	Individual	28
MoS_2/rGO	GCE	-	-	42.91 (μA/μM)	1.04 ppb	-	-	Yes	Individual	29
Poly (L-glutamic acid)/GO	GCE	7.29 (μA/μM)	1.68 ppb	-	-	8.95 (μA/μM)	1.52 ppb	Yes	Simultaneous	30
Carbon black/Polylactic acid	Drawn electrode	-	11.24 ppb	-	2.49 ppb	-	-	Yes	Simultaneous	31
PEDOT/PVA/AgNPs	SPCE	0.179 (μA/ppb)	3 ppb	0.171 (μA/ppb)	8 ppb	-	-	No	Simultaneous	32
Graphene/Polylactic acid	3D printed electrode	-	Unmeasureble below 44.96 ppb		Unmeasureble below 82.88 ppb	-	-	Yes	Simultaneous	33
		0.26 (μA/ppb)	9 ppb	0.28 (μA/ppb)	3 ppb	-	-	No, with Bi addition		
$Ti_3C_2T_x$ nanoribbons	GCE	14.51 (μA/μM)	0.10 ppb	-	-	-	-	No	Individual	34
GSH	**SPCE**	**0.0017 (μAV /ppb)**	**15.28 ppb**	**0.036 (μAV /ppb)**	**10.62 ppb**	**0.027 (μAV /ppb)**	**6.37 ppb**	**Yes**	**Simultaneous**	**This study**
GSH	**SPCE**	**0.032 (μAV /ppb)**	**3.36 ppb**	**0.021 (μAV /ppb)**	**3.49 ppb**	**0.021 (μAV /ppb)**	**3.61 ppb**	**Yes**	**Individual**	**This study**

Reference

1 Q. Yang, B. Nagar, R. Alvarez-Diduk, M. Balsells, A. Farinelli, D. Bloisi, L. Proia, C. Espinosa, M. Ordeix, T. Knutz, E. De Vito-Francesco, R. Allabashi, A. Merkoçi, *ACS ES&T Water* **2021**, *12*, 2470.

2 J.-H. Hwang, X. Wang, D. Zhao, M. M. Rex, H. J. Cho and W. H. Lee, Electrochim. Acta, 2019, 298, 440–448.

3 S. B. Hočevar, I. Švancara, K. Vytřas and B. Ogorevc, Electrochim. Acta, 2005, 51, 706–710.

4 P. K. Sahoo, B. Panigrahy, S. Sahoo, A. K. Satpati, D. Li and D. Bahadur, Biosens. Bioelectron., 2013, 43, 293–296.

5 L. Shi, Y. Li, X. Rong, Y. Wang and S. Ding, Anal. Chim. Acta, 2017, 968, 21–29.

6 Z. Wang, H. Wang, Z. Zhang and G. Liu, Sensors Actuators B Chem., 2014, 199, 7–14.

7 S. Chaiyo, E. Mehmeti, K. Žagar, W. Siangproh, O. Chailapakul and K. Kalcher, Anal. Chim. Acta, 2016, 918, 26–34.

8 M. A. Tapia, C. Pérez-Ràfols, R. Gusmão, N. Serrano, Z. Sofer and J. M. Díaz-Cruz, Electrochim. Acta, 2020, 362, 137144.

9 X. Niu, Z. Mo, R. Hu, H. Gao and Z. Li, J. Mater. Sci. Mater. Electron., 2017, 28, 9634–9641.

10 S. M. Choi, D. M. Kim, O. S. Jung and Y. B. Shim, Anal. Chim. Acta, 2015, 892, 77–84.

11 F. Pan, C. Tong, Z. Wang, H. Han, P. Liu, D. Pan and R. Zhu, Microchim. Acta, 2021, 188, 295.

12 N. Ruecha, N. Rodthongkum, D. M. Cate, J. Volckens, O. Chailapakul and C. S. Henry, Anal. Chim. Acta, 2015, 874, 40–48.

13 S. A. Hashemi, S. Bahrani, S. M. Mousavi, N. Omidifar, M. Arjmand, K. B. Lankarani and S. Ramakrishna, Eur. Polym. J., 2022, 162, 110926.

14 Jyoti, R. Kaur, Komal, Renu, P. Singh, N. Kaur, S. Rana and S. Singhal, Microchim. Acta, 2022, 189, 186.

15 V. Suvina, S. M. Krishna, D. H. Nagaraju, J. S. Melo and R. G. Balakrishna, Mater. Lett., 2018, 232, 209–212.

16 X. Guo, R. Cui, H. Huang, Y. Li, B. Liu, J. Wang, D. Zhao, J. Dong and B. Sun, J. Electroanal. Chem., 2020, 871, 114323.

17 T. Priya, N. Dhanalakshmi, S. Thennarasu, V. Karthikeyan and N. Thinakaran, Chem.

Phys. Lett., 2019, 731, 136621.

18 R. Fu, P. Yu, M. Wang, J. Sun, D. Chen, C. Jin and Z. Li, Microchem. J., 2020, 157, 105076.

19 X. Sun, M. Duan, R. Li, Y. Meng, Q. Bai, L. Wang, M. Liu, Z. Yang, Z. Zhu and N. Sui, Anal. Chem., 2022, 94, 13598–13606.

20 S. Liu, T. Wu, F. Li, Q. Zhang, X. Dong and L. Niu, Anal. Methods, 2018, 10, 1986–1992.

21 K. Krishna Kumar, M. Devendiran, P. Senthil Kumar and S. Sriman Narayanan, Environ. Res., 2021, 202, 111707.

22 X. Wang, W. Gao, W. Yan, P. Li, H. Zou, Z. Wei, W. Guan, Y. Ma, S. Wu, Y. Yu and K. Ding, ACS Appl. Nano Mater., 2018, 1, 2341–2346.

23 L. Yu, Q. Zhang, B. Yang, Q. Xu, Q. Xu and X. Hu, Sensors Actuators B Chem., 2018, 259, 540–551.

24 S. Duan and Y. Huang, J. Electroanal. Chem., 2017, 807, 253–260.

25 J. Shang, F. Xue, E. Ding, *Chem. Commun.* **2015**, *51*, 15811.

26 G. Bjørklund, G. Crisponi, V. M. Nurchi, R. Cappai, A. B. Djordjevic, J. Aaseth, *Molecules* **2019**, *24*, 3247.

27 T.-L. Ho, *Chem. Rev.* **1975**, *75*, 1.

28 B. A. Getachew, D. S. Bergsman, J. C. Grossman, *ACS Appl. Mater. Interfaces* **2020**, *12*, 48511.

29 Y.-F. Sun, J.-H. Sun, J. Wang, Z.-X. Pi, L.-C. Wang, M. Yang, X.-J. Huang, *Anal. Chim. Acta* **2019**, *1063*, 64.

30 W. Yi, Z. He, J. Fei, X. He, *RSC Adv.* **2019**, *9*, 17325.

31 F. M. de Oliveira, E. I. de Melo and R. A. B. da Silva, *Sensors Actuators B Chem.*, 2020, **321**, 128528.

32 U. Ngoensawat, T. Pisuchpen, Y. Sritana-anant, N. Rodthongkum and V. P. Hoven, *Talanta*, 2022, **241**, 123253.

33 J. G. Walters, S. Ahmed, I. M. Terrero Rodríguez and G. D. O'Neil, *Electroanalysis*, 2020, **32**, 859–866.

34 Y. Yi, Y. Ma, F. Ai, Y. Xia, H. Lin and G. Zhu, *Chem. Commun.*, 2021, **57**, 7790–7793.